Helicons in Unbounded Plasmas

R. L. Stenzel* and J. M. Urrutia
Department of Physics and Astronomy, University of California, Los Angeles, California 90095-1547, USA
(Received 5 March 2015; published 21 May 2015)

Helicons are whistler modes with helical phase fronts. They have been studied in solid state plasmas and in discharge tubes where boundaries and nonuniformities are ever present. The present work shows that helicons also exist in unbounded and uniform plasmas, thereby bridging the fields of laboratory and space plasma physics. First measurements of helicon field lines in three dimensional space are presented. Helicons with negative and positive mode numbers can propagate with equal amplitudes.

DOI: 10.1103/PhysRevLett.114.205005 PACS numbers: 52.35.Hr, 52.40.Fd, 52.50.Qt, 94.05.Rx

Magnetic field topologies are an important topic in plasma physics. They play a role in fusion devices, space plasmas, astrophysics, and electromagnetic waves. Whistler modes are electromagnetic waves in magnetized plasmas which have been known for a long time in space plasmas [1]. They are usually understood in terms of plane waves, but every real wave is a wave packet with a wave number spectrum [2]. For example, helicon waves have wave numbers in the azimuthal direction, radial direction, and parallel direction along the ambient field $\mathbf{B}_0$. They have been studied in solid state plasmas [3] and in gaseous plasma columns [4], which opened up many applications [5,6]. In spite of a vast body of literature on helicons, no measurements of magnetic field lines have been reported, partly because *in situ* field line measurements are impossible in solid state plasmas or space plasmas. This Letter describes field line measurements in large laboratory plasmas free of boundary effects [7,8]. Helicons, contrary to their name, have only a subset of helical field lines, while most lines are transverse as in circularly polarized whistler modes. Here, we will show that positive and negative helicons exist in uniform plasmas free of boundaries. This is contrary to most helicon experiments and theories which consider helicons to be waveguide eigenmodes of a small plasma column. We will show that, in the absence of radial boundaries, the properties of antennas determine the field topology. Radial propagation also enters into the field topology in unbounded plasmas.

Based on the observation of helicon modes in a large unbounded laboratory plasma, one can predict that helicons also exist in space plasmas. Active experiments with antennas will surely produce helicon modes in the ionosphere. Whistlers in narrow ducts are also helicons. Oscillating flux ropes in the whistler regime also have helicon topologies. Thus, the present Letter suggests a bridge between space plasma physics and application-oriented laboratory research on helicon devices. Magnetic antennas play an important role in both fields. For example, we show that the excitation of left and right handed helicons depends on the type of antenna and not, as presently thought, on the polarization properties of whistlers. Helicons with either sense of rotation are equally strong when excited with the proper antenna.

The experiments are performed in a large discharge device, few of which exist in the world, and are dedicated to whistler mode studies [9,10]. Our device produces a pulsed plasma of density $n_e \simeq 10^{11}$ cm^{-3}, electron temperature $kT_e \simeq 2$ eV, uniform axial magnetic field $B_0 = 5$ G in a large chamber (1.5 m diam, 2.5 m) filled with 0.4 mTorr Argon. Figure 1 shows a picture of the interior of the plasma device, depicting the heated cathode, the purple argon plasma, and antennas for exciting whistler modes. The single loop of 4 cm diam can be rotated with its dipole moment along $\mathbf{B}_0$ ($m = 0$ loop) or across $\mathbf{B}_0$ ($m = 1$ loop). For these configurations, the wave fields $\mathbf{B}_{\rm rf}$ have been measured with an electrostatically shielded triple magnetic probe movable in the y-z and x-y planes. The frequency is chosen at $f = 5$ MHz or $f/f_c = 0.357$ when normalized to the electron cyclotron frequency. The normalized collision frequency is $\nu_{e,\rm tot}/\omega_c \simeq 0.014$ where $\nu_{e,i} \gg \nu_{e,n}$.

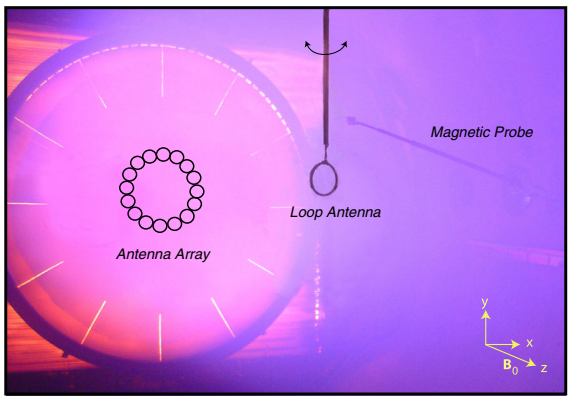

FIG. 1 (color online). Picture of the discharge plasma produced by a 1 m diam oxide coated cathode. A 4 cm diam loop antenna is inserted down into the uniform plasma center to excite helicon modes. A circular array for exciting $\pm m$ helicons is shown schematically.

The wave amplitudes are small ($B < 0.1$ G) so that nonlinear effects do not arise. The pulsed discharge is repeated at a rate of 1 Hz, the rf waveform is triggered at the same afterglow time and averaged over 10 shots so as to improve the signal-to-noise ratio. Since the discharge pulses are highly reproducible, one can obtain the field topology with a single probe with minimal plasma perturbations. The analog probe signals are digitized with a four-channel digital oscilloscope. Since we are interested in the field produced by plasma currents, the vacuum field of the antenna is measured on alternate shots and subtracted from the total field in the presence of plasma.

The linearity between antenna current and wave field has been established. It allows the superposition of fields from two or more antennas which has been verified earlier for counter-propagating whistler vortices [11]. Because of the uniformity in density and ambient magnetic field, it is also valid to shift the antenna with its wave field to a different position. By adding the fields of two separated loops, new antenna patterns can be generated. This concept can be extended to multiple antennas, e.g., multipole antennas, twisted antennas, and antenna arrays, to predict their radiation properties. Phasing orthogonal loops produces circularly polarized helicon fields.

A loop with a dipole moment along $\mathbf{B}_0$ excites an $m = 0$ helicon mode. It is a succession of whistler vortices of alternating signs. Each half wavelength section has a field-aligned dipolar field linked by an azimuthal field B_{tor} with $\partial/\partial\phi = 0$. Adjacent vortices are separated by a 3D spiral null point. In an unbounded plasma, the vortices propagate both radially and axially, which is manifested by oblique phase fronts in the component $B_z(y, z)$ and $B_x(y, z)$ shown in Figs. 2(a) and 2(b). The normal to the phase front shows that the phase velocity makes an angle $\theta \simeq 45°$ with respect to $\mathbf{B}_0$ which is close to the angle of the Gendrin mode $\theta_{\mathrm{G}} = \arccos(2\omega/\omega_c) = 44°$ [2,12]. This mode has a parallel group velocity which equals the parallel phase velocity. In time, the wave pattern propagates with constant velocity $v_{\parallel} \simeq 70$ cm/μs along $\mathbf{B}_0$, while the phase propagates obliquely with decreasing amplitude. Such modes have also been studied in bounded helicon devices [13,14], although the focus was on the dispersion characteristics rather than the field topology.

The field components have also been measured in the x-y plane. The constant axial propagation speed ($v = z/t$) allows us to construct the phase fronts and vector fields in 3D space. Figure 2(c) shows that isosurfaces of $B_z(x, y, z)$, i.e., the phase fronts, are conical. The field lines are tangential to the phase fronts ($\mathbf{k} \cdot \mathbf{B} = 0$) and, hence, are confined within each half-wavelength section. The vortex spine is along the axis, spiral fans arise close to the null points [Fig. 2(d)].

When the dipole moment of the loop antenna is oriented across $\mathbf{B}_0$, an $m = 1$ helicon mode is excited. This is the typical arrangement in helicon devices. Figure 3(a) describes, schematically, how the antenna excites the wave

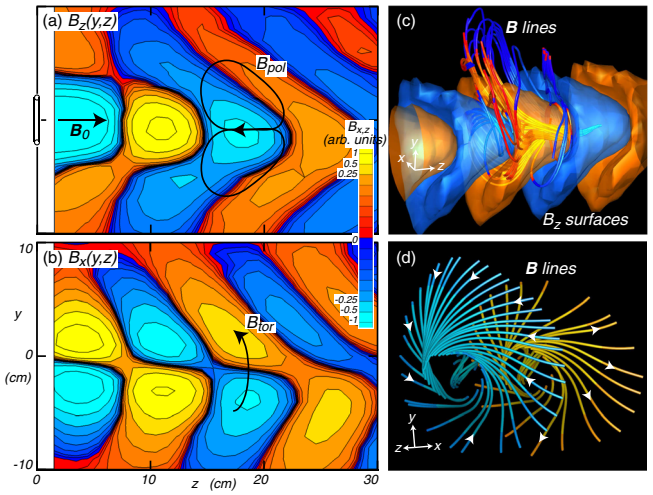

FIG. 2 (color online). Measured fields of an $m = 0$ whistler mode. (a) Contours of the axial field component $B_z(y, z)$ in arbitrary units (arb. units) excited by a dipolar field from the loop antenna. It is the axial component of a poloidal field of a vortex (see black line). (b) Contours of the azimuthal field $B_x(y, z)$ which forms a toroidal field in the x-y plane (see black line). The poloidal and toroidal fields are linked, which produces positive magnetic helicity. (c) 3D view of the semitransparent conical isosurfaces of B_z with embedded field lines. The field lines are confined to half wave sections of opposite field directions. On the central axis spiral null points are formed where $B_z \simeq 0$. (d) 3D field lines in sections of positive and negative B_z showing field line spirals with opposite directions but same right-handed field line rotation or positive helicity. The color of the lines reflects the sign of B_z. Here, arb. units stands for arbitrary units.

fields. The time-varying current in the loop gives rise to an inductive electric field around the loop. Along $\mathbf{B}_0$, the inductive field is opposed by a space charge field leaving a very small Ohmic electric field. Across $\mathbf{B}_0$, the space charge field adds to the inductive field, which gives rise to an electron Hall current J_x of opposite signs on the right and left sides of the loop. The opposing currents form an out-of-plane current loop which produces a B_y component. This induced current does not shield the antenna field but rotates it from B_x to B_y. The convection equation $\partial\mathbf{B}/\partial t = \nabla \times (\mathbf{v} \times \mathbf{B})$ predicts that the field convects along $\mathbf{B}_0$, which creates the propagating wave.

Figure 3(b) shows, schematically, the induced plasma fields which have propagated away from the antenna. It is helpful to decomposes the 3D fields into linked field lines which form transverse dipole fields whose dipole moments rotate in ϕ direction around $\mathbf{B_0}$. In order to close the transverse dipolar field lines, an axial field B_z is needed. It peaks off the z axis and has opposite directions on either side of the transverse dipole field. The dipole fields are linked, which produces positive (negative) magnetic helicity for propagation along (against) $\mathbf{B_0}$.

The schematic picture is confirmed by measured field components displayed in Figs. 3(c) and 3(d) for two

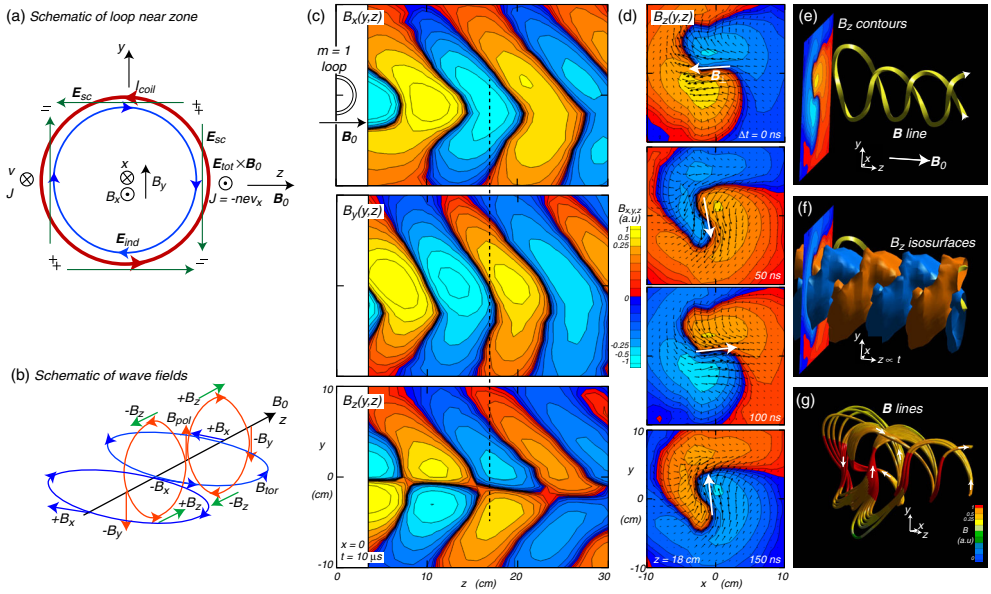

FIG. 3 (color online). Properties of $m = 1$ whistler modes. (a) Schematic picture of fields and currents near a loop antenna with dipole moment across $\mathbf{B}_0$. (b) Schematic picture of the wave fields decomposed into linked loops for purpose of simplification. (c) Contours of the three measured field components in the y-z plane of the loop ($x = 0$). The V-shaped phase fronts indicate oblique propagation in the Gendrin mode. The B_x and B_y components are shifted by $\lambda/4$ indicating circular polarization. (d) Contours of the axial field component B_z and vector field of (B_x, B_y) in the x-y plane at different times within one rf period. The field rotates in the same sense and rate as electrons rotate around $\mathbf{B_0}$, i.e., clockwise in space. (e) Selected 3D field line for an $m = +1$ helicon mode which forms two left-handed spiraling helices of opposing field line direction with closure at left side. (f) Isosurfaces of $B_z = \text{const}$ indicating the helical phase fronts of a helicon mode. Field lines lie inside the phase fronts. (g) Multiple 3D field lines started in different x-y planes, showing field line closure and formation of the helical spirals. On the left side, the spiral closes via transverse fields through the axis. As the starting plane is shifted in z, the transverse field rotates consistent with circular polarized whistlers. Off axis, the field lines are guided by the rotating B_z field into spirals tangential to the phase fronts or isosurfaces. The color of the field lines indicates the field strength which peaks near the axis of the spirals.

orthogonal planes. V-shaped phase fronts are observed in all components. The transverse components are circularly polarized. The axial component has two off-axis extrema which rotate together with the transverse field counter clockwise in the x-y plane. The V-shaped phase contours produce radially outward spiraling phase contours in the x-y plane.

Figures 3(e) and 3(f) show field lines and isosurfaces in 3D space. The phase of cylindrical helicon waves varies as $e^{i(m\phi+kz-\omega t)}$. The azimuthal propagation creates the rotation in ϕ, the axial propagation creates spiraling phase fronts seen in the isosurfaces of B_z, and the radial propagation produces spiral arms for the phase fronts in the x-y plane. Except for the radial propagation, the wave is an $m = +1$ helicon mode. We note that the antenna field is oscillating $[\propto \cos(m\phi)\cos(\omega t)]$ but not rotating $[\propto \cos(m\phi - \omega t)]$. The antenna field could excite both $m = +1$ and $m = -1$ modes, but the latter is not observed in many previous experiments and is considered a remaining puzzle [6].

We demonstrate that, with a different antenna, both $m = \pm 1$ modes can be excited. By placing two $m = 0$ loops of opposing polarity next to each other in an x-y plane at $z = 0$, the bipolar B_z components of an $m = 1$ helicon mode are excited. The superposition of two $m = 0$ helicons also produces a dipolar field in the transverse field components. Again, the antenna field is not rotating but forms a standing wave in the azimuthal direction. Figure 4(a) displays 3D field lines and B_z isosurfaces of the excited modes. The B_z components propagate without rotating and, hence, can be decomposed into two oppositely

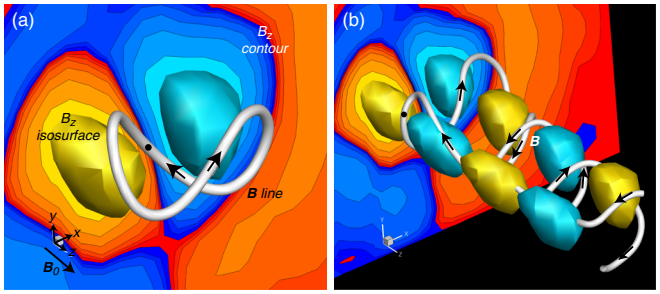

FIG. 4 (color online). Field lines and B_z components of a dipole field generated by two adjacent $m = 0$ loop antennas. (a) $B_z(x, y)$ contours and isosurfaces and a closed field line in an axial half wavelength segment of the wave train. The field line is traced from a point near a null in B_z. (b) Multiple isosurfaces showing no rotation of B_z which can be considered a superposition of $m = 1$ and $m = -1$ modes. A field line is launched at the peak of B_z and meanders through the isosurfaces along the whole wave train. The transverse B vector on axis rotates left handed in space or right handed in time appropriate for whistlers. Thus, the helicon can be considered an $m = \pm 1$ mode.

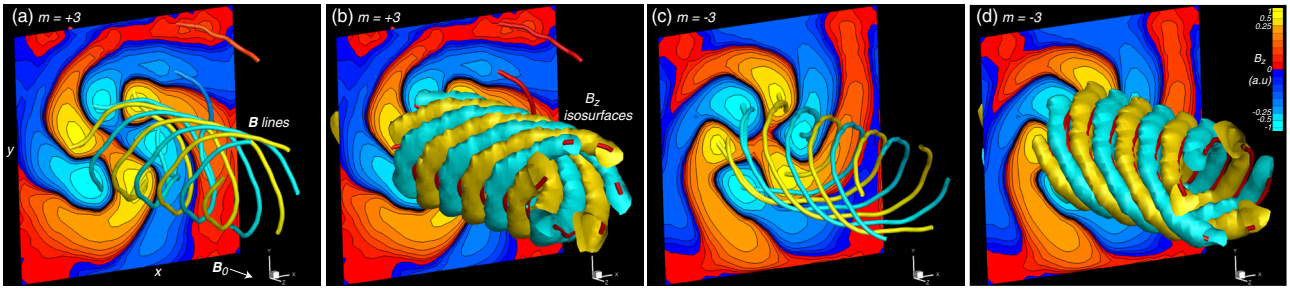

FIG. 5 (color online). Rotating field of a hexapole antenna exciting $m = \pm 3$ helicon modes. (a) Contours of $B_z(x, y)$ and 3D field lines showing six left-handed spirals characteristic for an $m = +3$ helicon. (b) Isosurfaces $B_z(x, y, z) = \text{const}$ showing spiraling phase fronts of the propagating helicon wave. The pitch is three axial wavelengths. Field lines are nearly parallel to the phase front. (c) Same as (a) but with reverse rotation of the antenna field. It creates an $m = -3$ helicon mode which is just as strong as the $m = 3$ mode. (d) Same as (b) but for clockwise rotation which produces an $m = -3$ helicon.

rotating modes of equal amplitudes. The field lines do not form a circular spiral but meander from one B_z peak to another. The oscillating field line does not describe the general field topology. Figure 4(b) shows a field line launched on axis between the B_z extrema. It forms a figure eight and closes within the half-wavelength section shown. Because of the B_z components, the figure eight is axially stretched and does not intersect. On axis, the transverse field rotates and, together with the meandering field line, forms a circularly polarized field. This example shows that equally strong $m = 1$ and $m = -1$ helicons are excited by a different antenna than the $m = 1$ loop.

In order to selectively excite positive or negative helicon modes, a rotating antenna field is required. This can be done with crossed and phased $m = 1$ loops or pairs of rotated and phased $m = 0$ loops. In order to excite higher order m modes, we investigate the wave excitation from a circular array of 16 $m = 0$ loops. The array is phased so as to create a circularly traveling wave. For an integer number of wavelengths around the array, we have an m-mode antenna. Modes from $m = 0$ to $m = 8$ have been created. Earlier, we have shown that a phased linear array excites oblique plane waves [8]. For the present circular array, the waves are oblique on a cylindrical $\phi - z$ surface, i.e., helical waves.

Figure 5 shows the topology of $m = \pm 3$ helicons. In the x-y plane at 18 cm from the antenna, the B_z component forms a hexapole configuration. The B_z contours exhibit spiral arms due to the outward radial propagation. Fig. 5(a) shows field lines launched in the B_z extrema. These form six nested helices, three with forward field lines, three with return field lines, each with a pitch of three wavelengths. Figure 5(b) shows isosurfaces of B_z, which indicate helical phase fronts with embedded field lines. In Figs. 5(c) and 5(d) the sense of rotation has been reversed. There is no difference in amplitude or propagation speed between the $m = +3$ and $m = -3$ helicon modes. Both are oblique whistler modes whose field vectors are right hand circularly polarized in time.

When rotating fields are produced by crossed $m = 1$ loops, the negative m modes are usually weak and lack spiral field lines. The reason is that the antenna couples to the transverse field components and relies on the plasma to develop the B_z component. When the antenna field rotates clockwise (cw), it cannot not excite a right handed whistler mode; hence, neither develops a cw rotating B_z component nor spiraling field lines.

In summary, we have shown the 3D field topologies of helicon modes in a uniform plasma without boundary effects. Helicons with mode number m have m pairs of helical field lines. Most field lines are not helical. Antennas determine mode numbers. Negative and positive mode numbers can be excited equally with suitable antennas. Radial propagation occurs in unbounded plasmas. The antenna does not radiate waves along the group velocity cone which is typical for small antennas [15,16]. Trivelpiece-Gould modes are not observed in a dense and uniform plasma. These new findings are relevant to the physics of whistler modes in areas ranging from helicon discharges to space plasmas.

The authors gratefully acknowledge support from National Science Foundation Grant No. 1414411.

*stenzel@physics.ucla.edu;
http://www.physics.ucla.edu/plasma-exp/

[1] H. Barkhausen, Zwei mit Hilfe der neuen Verstaerker entdeckte Erscheinungen, Phys. Z. **20**, 401 (1919).
[2] R. A. Helliwell, *Whistlers and Related Ionospheric Phenomena* (Stanford University Press, Stanford, CA, 1965).
[3] C. R. Legendy, Macroscopic theory of helicons, Phys. Rev. **135**, A1713 (1964).
[4] J. P. Klozenberg, B. McNamara, and P. C. Thonemann, The dispersion and attenuation of helicon waves in a uniform cylindrical plasma, J. Fluid Mech. **21**, 545 (1965).
[5] A. J. Perry, D. Vender, and R. W. Boswell, The application of the helicon source to plasma processing, J. Vac. Science **9**, 310 (1991).
[6] F. F. Chen, Helicon discharges and sources: a review, Plasma Sources Sci. Technol. **24**, 014001 (2015).

[7] J. M. Urrutia and R. L. Stenzel, Magnetic antenna excitation of whistler modes. i. basic properties, Phys. Plasmas **21**, 122107 (2014).

[8] R. L. Stenzel and J. M. Urrutia, Magnetic antenna excitation of whistler modes. ii. antenna arrays, Phys. Plasmas **21**, 122108 (2014).

[9] A. V. Kostrov, A. V. Kudrin, L. E. Kurina, G. A. Luchinin, A. A. Shaykin, and T. M. Zaboronkova, Whistlers in thermally generated ducts with enhanced plasma density: excitation and propagation, Phys. Scr. **62**, 51 (2000).

[10] W. E. Amatucci, Whistler Wave Resonances in a Laboratory Plasma, IEEE Trans. Plasma Sci. **39**, 637 (2011).

[11] J. M. Urrutia, R. L. Stenzel, and M. C. Griskey, Laboratory studies of magnetic vortices. iii. collisions of emhd vortices, Phys. Plasmas **7**, 519 (2000).

[12] R. Gendrin, Le guidage des whistlers par le champs magnetique, Planet. Space Sci. **5**, 274 (1961).

[13] C. M. Franck, O. Grulke, and T. Klinger, Transition from unbounded to bounded plasma whistler wave dispersion, Phys. Plasmas **9**, 3254 (2002).

[14] C. M. Franck, R. Kleiber, G. Bonhomme, O. Grulke, and T. Klinger, Transition from unbounded to bounded whistler wave dispersion: Reconsidered, Phys. Plasmas **10**, 3817 (2003).

[15] R. L. Stenzel, Antenna radiation patterns in the whistler wave regime measured in a large laboratory plasma, Radio Sci. **11**, 1045 (1976).

[16] A. W. Degeling, G. G. Borg, and R. W. Boswell, Transitions from electrostatic to electromagnetic whistler wave excitation, Phys. Plasmas **11**, 2144 (2004).